Detection of the farm road positioning scene classification for unmanned driving based on GNSS

Banghao Lin[1], Caicong Wu[1], Wei Song[1*], Hasan Abdulhussein Jaafar[2]

(1. *College of Information and Electrical Engineering, China Agricultural University, Beijing 100083, China*;
2. *Faculty of Engineering, University of Kufa, Kufa 54003, Iraq*)

Abstract: The positioning environment of farm roads is complex and variable, with defined scenes including open sky, forest, overpass, and tunnel. Relying solely on the Global Navigation Satellite System (GNSS) for positioning throughout the operation of unmanned agricultural machines is insufficient. This study addressed the need for rapid and accurate identification of farm road scene types to select appropriate positioning devices for unmanned agricultural machines. Real-time satellite signal data, obtained through onboard GNSS receivers and combined with broadcast ephemeris data, were used to extract positioning status and track satellite statistics and distribution features. A classifier based on a sliding window was developed, and an inference based on tracked satellite numbers was proposed to detect the farm road positioning scene and calculate the length of different road segments. This study was conducted using real-world working conditions at an agricultural machinery cooperative in Miyun, Beijing, China, where three sets of GNSS data were collected from the farm road using a vehicle-mounted all-frequency GNSS receiver. The results showed that the classification accuracy for open-sky, overpass, and tunnel scenes was 93.96%, with a recall rate of 98.31% and an F1 score of 95.82%. Compared with random forest and XGBoost, the F1 scores improved by 17.83 and 5.70, respectively. This method, based on GNSS multi-feature fusion, can provide a reference for selecting multi-source positioning devices and planning the routes of unmanned agricultural machines.

Keywords: farm road, feature fusion, GNSS, scene detection, unmanned driving

DOI: 10.25165/j.ijabe.20261902.9654

Citation: Lin B H, Wu C C, Song W, Jaafar H A. Detection of the farm road positioning scene classification for unmanned driving based on GNSS. Int J Agric & Biol Eng, 2026; 19(2): 226–234.

1 Introduction

In the agricultural field, environments are typically characterized by open sky, with protective forests only around the periphery[1]. In such open positioning scenes, agricultural machines can achieve high-precision and reliable positioning, navigation, and control by using only the Global Navigation Satellite System (GNSS) and Continuously Operating Reference Station (CORS) systems, enabling either assisted or autonomous driving of high accuracy and reliability[2-4]. However, unmanned agricultural machines usually operate in complex and diverse environments when moving between depots, farm roads, and fields, with positioning environments on farm roads particularly challenging. These environments often include open sky, forest, overpass, and tunnel scenes, where using only GNSS data for positioning and navigation is insufficient in terms of reliability[5,6].

Thus, it is critical to quickly and accurately identify the positioning environment of farm roads to provide appropriate recommendations for selecting suitable positioning devices for unmanned agricultural machines. Visual sensors are commonly used for scene recognition in urban traffic, but this is not suitable for agricultural environments. Autonomous agricultural work often extends into nighttime conditions. Unlike urban areas with street lighting, nighttime farmland is only illuminated by vehicle headlights. These headlights cannot fully illuminate the surrounding environment, which poses a significant challenge for scene recognition algorithms based on visual sensors. GNSS sensors, with their all-weather and wide-area coverage advantages, are largely unaffected by agricultural environments, making them more suitable for this context.

Many studies use GNSS receivers for positioning context analysis of various scenarios. Two common methods for assessing positioning and navigation signal obstructions are based on satellite visibility and receiver signal data. The first method quantifies different levels of signal obstruction across various locations. For instance, Kou et al.[7] constructed sky obstruction boundaries using panoramic images and calculated the GNSS satellite visibility in urban road areas, enabling temporal and spatial visibility evaluations of the satellites. Xu et al.[8] used a smoothing spline model to estimate sky contours based on satellite visibility maps, computing obstruction profiles for buildings by an adaptive weighting scheme. Kim et al.[9] employed digital surface models from drone mapping technologies to assess signal shadowing due to surrounding obstacles at specific locations. Kou et al.[10] further extended this approach by utilizing airborne laser scanning point clouds to analyze GNSS signal attenuation caused by trees, enabling more precise visibility analysis in forest environments. These methods primarily focus on depicting the visible sky above the receiving antenna to quantify the number of visible satellites, reflecting the accuracy of GNSS positioning at different locations. However, such models are only applicable over short periods, especially in dynamic environments

Received date: 2025-01-23 **Accepted date:** 2026-01-13

Biographies: Banghao Lin, MS, research interest: autonomous operation and precision agriculture, Email: lbanghao@126.com; **Caicong Wu**, PhD, Professor, research interest: unmanned driving and autonomous operation of agricultural machinery, big data mining of agricultural machinery, Email: wucc@cau.edu.cn; **Hasan Abdulhussein Jaafar**, PhD, Professor, research interest: geodesy and surveying, Email: Hasan.Jaafar@nottingham.ac.uk.

***Corresponding author: Wei Song**, PhD, Postdoctor, research interest: position, navigation, and timing in agriculture. College of Information and Electrical Engineering, China Agricultural University, No.17 Qinghua East Road, Haidian District, Beijing 100083, China. Tel:+86-18811051719, Email: songw@cau.edu.cn.

like forests, where seasonal changes affect signal visibility. The second method evaluates the GNSS signal quality to infer potential positioning obstructions in the current environment. For example, Zhang et al.[11] developed a parametric model to match the tracked satellite's elevation and azimuth angle, considering pseudo-random noise, achieving the identified scene segment recognition of 4.38% average deviation in railway environments. Similarly, Chen et al.[12] used signal characteristics that are the number of visible satellites and signal-to-noise ratio, to classify underwater navigation scenes with a K-means clustering accuracy of 90.40%. By using carrier-to-noise ratios (CNR) and horizontal dilution of precision, Liang et al.[13] applied a four-state Markov chain model to reconstruct environments and designed a two-stage iterative matching algorithm to segment GNSS data and identify the scene of each segment, achieving an overall classification accuracy of 97.08%. Xia et al.[14] employed recurrent neural networks (RNN), with the number of visible satellites, satellite signal CNR, and its statistical value, to recognize transitions between indoor and outdoor scenes, and the overall recognition accuracy reached 98.65%. These methods primarily use the distribution of GNSS satellites and signal quality to identify the current obstruction scene, supporting the development of positioning strategies. Scene descriptions provide semantic information about how the obstruction environment impacts positioning. By inferring the positioning conditions from the scene type, we can offer strategic insights for device selection. Although this method is not as accurate as the modeling analysis, it is more effective for the description of the long-timescale and the formulation of the positioning scheme.

In this study, the GNSS satellite statistical features and distribution features were extracted from the data output by GNSS receivers, using a scene classification method based on sliding windows and a random forest algorithm, and a U-turn segment method was proposed for tracking the tracked satellite number. The method calculates the length of different road segments under various scene types and provides information to farm administrators for selecting appropriate positioning devices and planning routes for unmanned agricultural machines. The workflow of this study is shown in Figure 1.

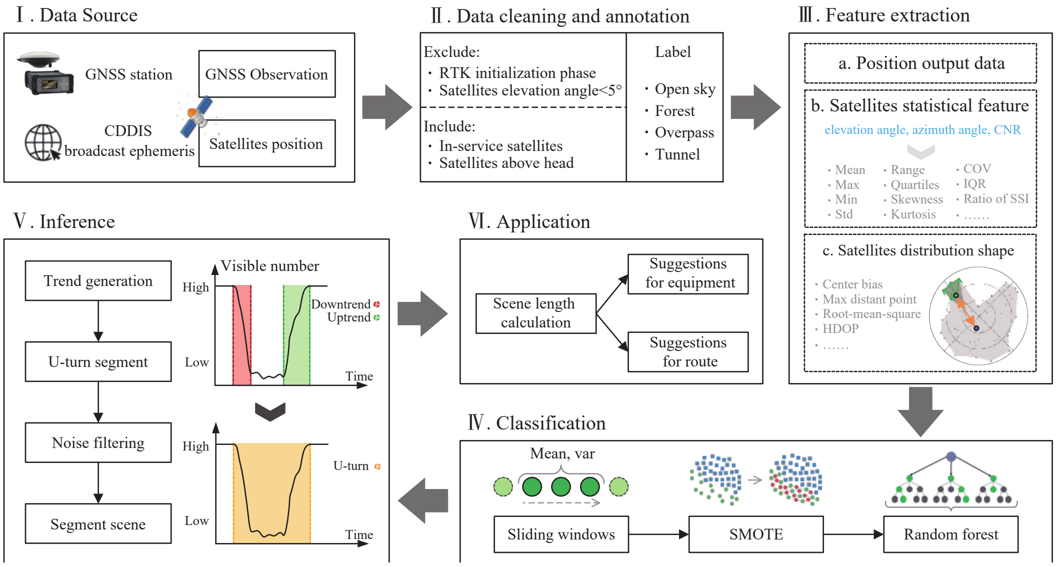

Figure 1 Workflow of the GNSS-based detection method

2 Materials and methods

2.1 Data collection

2.1.1 Experimental scenes

Farm roads are the paths agricultural machinery uses to shuttle between depots and fields, primarily distributed in suburban and rural areas. Unlike urban roads, farm roads are generally surrounded by low vegetation rather than tall structures. Based on common factors affecting positioning on farm roads and referencing the classification methods proposed by Groves et al.[15] and Feriol et al.[16], four types of farm road positioning scenes (Figure 2) were defined in this study. The details are as follows:

Open sky: Farm roads are surrounded by open fields, low walls, or shrubs, allowing the GNSS receiver to capture signals from many satellites in direct line of sight. Multipath effects are minimal, and GNSS positioning performs well, characterized by a high number of visible satellites and high positioning accuracy, continuity, and reliability.

Forest: Farm roads are flanked by trees with overhead canopies (dense in seasons other than winter), partially obscuring the sky. The GNSS receiver detects many non-line-of-sight signals, and multipath effects are significant, negatively impacting the accuracy, continuity, and reliability of GNSS positioning[17].

Overpass: An overpass (road or railway) crosses over the farm road, allowing the GNSS receiver to capture signals from satellites at low elevation angles. Line-of-sight signals are severely attenuated, and the positioning accuracy, continuity, and reliability of GNSS are reduced.

a. Open sky b. Forest c. Overpass d. Tunnel

Figure 2 Farm road scenes classification

Tunnel: The farm road passes through a tunnel or culvert, completely blocking GNSS signals and resulting in positioning failure.

The experimental data were collected in Henanzhai Town, Miyun District, Beijing (40°20′24.30″N, 116°50′7.42″E), China, with a route of approximately 9 km. The route followed a "depot-farm road-field-farm road-depot" pattern (Figure 3). The data collection was performed three times along the same route at an average speed of approximately 20 km/h. The weather was clear during each data collection: once on March 6, 2024, for the test set, and twice on May 11, 2024, for training and validation sets, respectively.

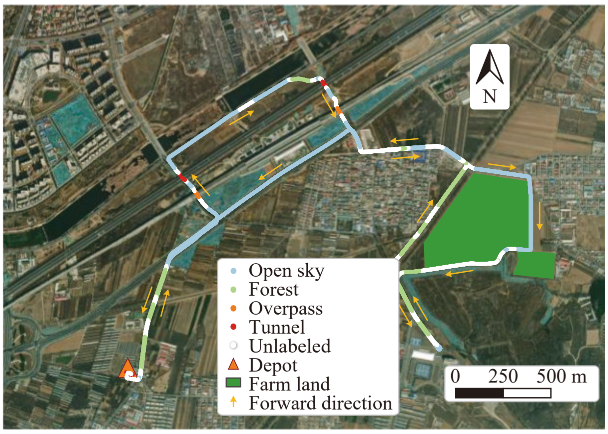

Figure 3 Data acquisition route and scene annotation

2.1.2 GNSS data collection

A high-precision GNSS receiver (model: UR4B0-D) was used, supporting all satellite constellations and frequencies, paired with an external multi-system full-frequency antenna (model: HX-CSX601A). The CORS data was obtained from the China Mobile High Precision Positioning Platform, which broadcasts network real-time kinematic (RTK) corrections with less than 3 cm accuracy. A video recording device (iPad) was used to capture footage of the sky and the scene ahead of the vehicle during data collection. The GNSS antenna was mounted at the center of the vehicle's roof, with the receiver placed inside the cabin (Figure 4). All data was recorded at 10 Hz and stored in NEMA-0183 GPGGA and NovAtel BESTPOS, BESTVEL, and RANGE formats.

2.1.3 Auxiliary data collection

The broadcast ephemeris data from the NASA Crustal Dynamics Data Information System (CDDIS)[18] were downloaded to obtain GNSS satellite ephemerides for the dataset dates. Using RTKLib, the satellite elevation and azimuth angles for GPS, BeiDou, Galileo, and GLONASS constellations were calculated for each location in the dataset. The satellite distributions during the data collection period are shown in Figure 5. Since most GNSS satellites are constantly moving relative to the ground, the distribution of data collected in different time periods is different. The training and validation sets had similar satellite distributions, whereas the test set showed a distinctly different distribution. The calculated satellite angles were used as auxiliary data for feature extraction.

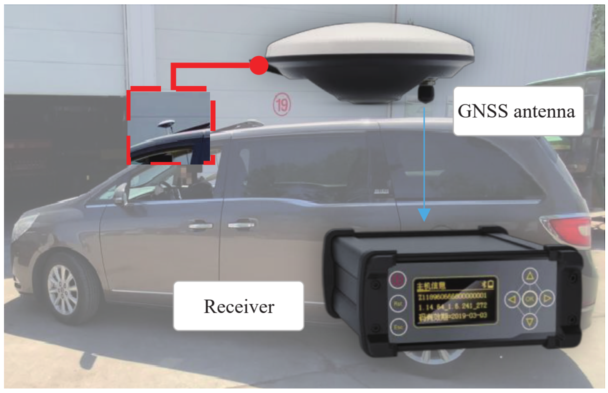

Figure 4 Equipment used for data collection

2.2 Data preprocessing

2.2.1 Data cleaning

The float RTK solution was excluded from the initialization phase because float solutions do not provide accurate positioning information, which could affect data annotation. The data points were also removed from satellites with an elevation angle of less than 5°, as satellites below this angle typically do not contribute to position calculation. Additionally, satellites that were out of service during the data collection period, as indicated by the ephemeris data, were excluded to avoid interference in the feature extraction process.

2.2.2 Data annotation

Using MapBox satellite imagery and the vehicle video recordings, the positioning scenes were annotated for each point in the dataset using geographic information software (QGIS Desktop 3.38.0). Transition points between different scenes, which were difficult to clearly define, were left unlabeled. Additionally, the test set did not include forest scenes due to the season (winter), during which the primary obstructing factor, tree leaves, was absent. Since the depot had a roof that created a tunnel-like environment, the positioning points in the depot were labeled as tunnel scenes. The annotated results are shown in Figure 3, with statistics listed in Table 1.

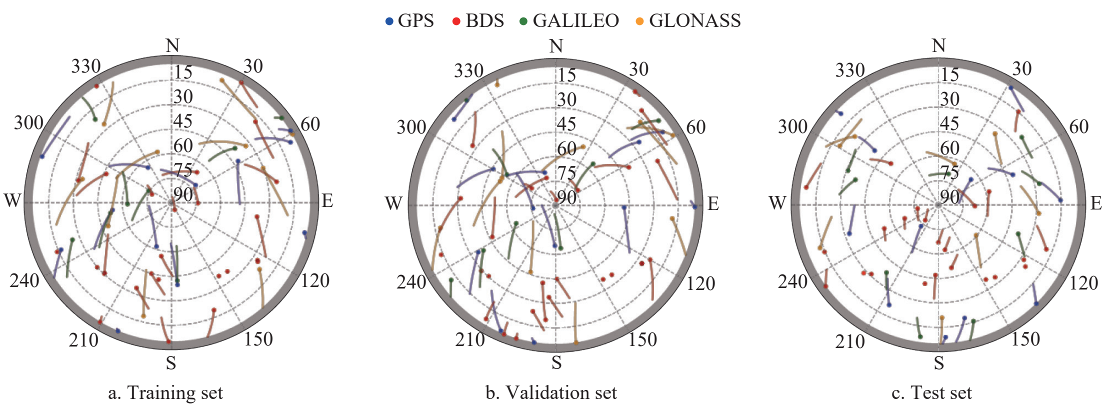

Figure 5 Distribution of GNSS satellites in the sky

2.3 Feature extraction

The extracted features are divided into three categories: Position output data, which comes from the GNSS receiver's BESTPOS text output; GNSS satellite statistical features, which are statistical calculations of satellite positions and signal strength; and GNSS satellite distribution features, which describe the sky plot of tracked satellites.

Table 1 A summary of dataset annotation

Dataset	Time (UTC+8)	Open sky	Forest	Overpass	Tunnel	Unlabeled
Training set (30 326 points)	11 May 11:59-12:49	7666	3036	114	2219	17 291
		25.29%	10.01%	0.38%	7.32%	57.02%
Validation set (30 694 points)	11 May 11:07-11:58	6870	2900	108	1433	19 383
		22.38%	9.45%	0.35%	4.67%	63.15%
Test set (19 453 points)	6 March 11:06-11:34	7726	-	104	1137	10 486
		39.72%	-	0.53%	5.84%	53.90%

2.3.1 Position output data

The positioning output data can be obtained directly from all GNSS receivers without additional processing. This provides a baseline for simple features. The BESTPOS data format not only provides the best position but also includes various receiver status indicators and positioning status information. The selected features include solution status, position type, latitude standard deviation, longitude standard deviation, altitude standard deviation, number of tracked satellites, number of satellites used for solution, number of satellites with L1/E1/B1 signals used in solution, number of satellites with multi-frequency signals used in solution, differential age in seconds, and solution age in seconds.

2.3.2 Satellite statistical features

To fully capture the characteristics of the received GNSS signals and reflect the signal strength and distribution under different scene types, we used the elevation angles, azimuth angles, and CNR of all tracked satellites to calculate various statistical measures, including the mean, standard deviation, maximum, minimum, range, quartiles, interquartile range, skewness, kurtosis, and coefficient of variation.

Additionally, to represent the level of environmental interference affecting GNSS signals, we calculated the ratio of tracked satellites to satellites in the sky and the ratio of satellites used for positioning to tracked satellites. Moreover, following the RINEX standard for Signal Strength Indicator (SSI), the proportion of satellites at different SSI levels relative to the total number of tracked satellites was calculated by us.

2.3.3 Satellite distribution features

To describe the sky obstruction under different scenes, the GNSS satellite distribution was treated as geometric shapes. The positions of the satellites in the sky were considered vertices of the shapes, and the CNR of the signal was used as the weight. The centroid and barycenter of the satellite distributions were calculated (shape A for tracked satellites and shape B for satellites in the sky), and the root-mean-square (RMS) and maximum distance between the centroid and vertices were subsequently determined, as well as the distance between these centers for shapes A and B. Additionally, the satellite distribution features included the horizontal dilution of precision (HDOP) data reported in GPGGA. All feature information is listed in Table 2.

Table 2 A summary of extracted features

Type	Feature description	Number
Position output data	Features (11): solution status, positioning type, standard deviation of latitude/longitude/altitude, number of tracked satellites, number of satellites used for solution, number of satellites with L1/E1/B1 signals used in solution, number of satellites with multi-frequency signals used in solution, differential age, solution age	11
Satellite statistical features	Parameters (3): elevation angle, azimuth angle, CNR Statistical features (11): mean, standard deviation, maximum, minimum, range, quartiles 25%, quartiles 75%, interquartile range, skewness, kurtosis, coefficient of variation Other features (11): ratio of received satellites to visible satellites, ratio of satellites used for positioning to received satellites, ratio of satellites in different SSI levels to total received satellites	$3\times11+11=44$
Satellite distribution features	Centers (2): centroid, barycenter Calculated features (5): position of centers in shape B, centers bias of shapes A and B, RMS of vertex distances from centers, maximum vertex distance from centers Other features (1): HDOP	$2\times5+1=11$

Note: SSI: Signal strength indicators are part of the code and phase observations to offer a compact quality indicator. The generation of the RINEX signal strength indicators sn_rnx in the data records (1 = very weak, …, 9 = very strong) are standardized.

2.4 Classification

The classification contains three steps (Figure 1). First, the sliding window extracts spatial variation information in a short range. Second, data oversampling compensates for minority class samples, enhancing model robustness. Third, the random forest algorithm classifies scene types. This approach effectively utilizes GNSS signal features to tackle the inherent complexity of farm road environments, such as open sky, forest, overpass, and tunnel, ensuring that agricultural machinery can adapt to the diverse challenges presented by these environments.

2.4.1 Sliding window

On the farm road, the transition between different scenes tends to be gradual, for example, from the open sky to the light forest to the dense forest. The use of sliding windows can effectively capture this gradual change of spatial information. To accommodate this change, we used a sliding window to capture the changing features of the GNSS data. In time series, the mean and variance of feature values for each point, along with two preceding and succeeding points, were calculated to represent the changing pattern of positioning signals. For points near the sequence boundaries, the window size is gradually reduced until it contains only the current point. Since boundary points account for only a tiny proportion of the data, their effect on the overall results is negligible.

The sliding window is particularly effective in environments like forests, where signal attenuation can gradually increase. By averaging the signal metrics over multiple points, this method ensures that classification decisions are made based on a broader context rather than isolated points, reducing the impact of noise and abrupt changes caused by brief obstructions. Additionally, this approach allows the model to smooth out minor fluctuations in GNSS signals, providing more reliable scene classification even in challenging agricultural environments.

2.4.2 Data oversampling

Due to the imbalance in the number of samples, such as overpasses and tunnels, across different scene types in the training set, directly using this data for model training would result in poor prediction performance. Therefore, we applied the Synthetic Minority Over-sampling Technique (SMOTE)[19]. This method identifies minority class samples in the dataset and then uses the K-nearest neighbors algorithm to compute Euclidean distance to other minority class samples. New samples are generated by interpolating between neighboring minority class samples. Especially in scenes such as overpasses and tunnels, oversampling effectively expands the scene data boundary, making the classification results of the model more accurate in these minority class scenes.

2.4.3 Random forest

Integrating random forest classification and sliding windows significantly enhances the model's robustness in handling the inherent variability of farm road environments. To determine suitable model settings, a grid search procedure was employed to explore combinations of key hyperparameters, including the number of trees, the feature selection strategy, and the maximum number of features considered at each split. The dataset was input into the model, and bootstrapping was used to create multiple sampling datasets, which were then used to train 140 base decision trees. At each node of the tree model, a random subset of features was selected, with the subset size equal to the square root of the total number of features (eight in this study). A feature was selected from this subset based on the logarithmic loss function to split the node. The process continued until no further splitting was possible or the tree construction was complete. The final classification result was determined by majority voting among all trees[20]. Random forests are particularly well-suited for this classification due to their capacity to manage high-dimensional feature spaces and mitigate overfitting, which is an essential requirement given the dynamic nature of agricultural settings.

2.5 Inference

A tracked satellite number-based inference is developed to find the whole segment of the overpass and tunnel scenes. The random forest-based classification may give false results because the boundaries of the scene change need context information. The key idea of inference is to find U-turn patterns, as shown in Figure 6. Based on this idea, the inference rules are developed from the perspective of scene-switching features.

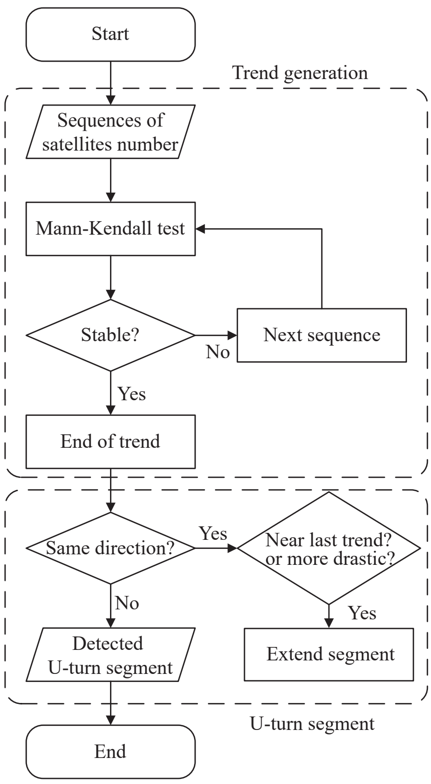

Figure 6 Workflow of the trend generation and U-turn segment

The road segment of the overpass and the tunnel can be divided into three parts: decreasing, stabilization, and increasing. The length of stabilization depends on the length of the obstruction. Due to high-frequency data collection, the tracked satellite number gradually decreases and increases when entering and leaving the scene of the overpass and tunnel. There are four steps in the tracked satellite number-based process. Firstly, trend generation finds a list of trends that obviously change the tracked satellite number. Secondly, the U-turn segment combines trends into a list of segments that start from the beginning of decreasing to the end of increasing. Thirdly, noise filtering filters out non-overpass and non-tunnel segments, and corrects overpass and tunnel outside segments. If the classification result point in a segment is less than a ratio, it is considered an accident fluctuation. Lastly, the segment scene is considered by the classification result point ratio in a segment. If the tunnel point in a segment is more than a ratio, all points in the segment will be classified as a tunnel, which is the same as the overpass scene.

2.5.1 Trend generation

Given a set of tracked satellite numbers X, x_i and x_j represent the number of tracking satellites at the i-th position and the j-th position respectively, and the Mann-Kendall method is chosen to test the stabilization in the time window because of its characteristics of non-parameter test and insensitivity to anomalies. For each time window, the null hypothesis H_0 indicates that the tracked satellite number is random and has no trend. If H_0 is rejected, the alternative hypothesis H_1 indicates the existence of a trend in the series. In this method, the difference between each number and all the numbers is calculated, and the parameter S is obtained. For a time-window containing n numbers, the estimator S can be calculated as follows:

$$S = \sum_{i=1}^{n-1} \sum_{j=i+1}^{n} \operatorname{sign}(x_i - x_j) \tag{1}$$

$$\operatorname{sign}\left(x_i - x_j\right) = \begin{cases} 1 & \text{if } x_i > x_j \\ 0 & \text{if } x_i = x_j \\ -1 & \text{if } x_i < x_j \end{cases} \tag{2}$$

When n numbers are more than eight, S almost follows the normal distribution, and its mean $E(S)$ and standard deviation $\operatorname{Var}(S)$ are determined by the following:

$$E(S) = 0 \tag{3}$$

$$\operatorname{Var}(S) = \frac{n(n-1)(2n+5)}{18} \tag{4}$$

$$z = \begin{cases} \dfrac{S-1}{\operatorname{Var}(S)} & \text{if } S > 0 \\ 0 & \text{if } S = 0 \\ \dfrac{S+1}{\operatorname{Var}(S)} & \text{if } S < 0 \end{cases} \tag{5}$$

where, z represents z statistic, which is a standardized Mann-Kendall test that follows a normal distribution and has a mean of 0 and a variance of 1.

2.5.2 U-turn segment

The standard normal variable from the trend indicates the trend direction. As shown in Figure 7, going through a tunnel at one time, the tracked satellite number will show a U-turn (tunnel)- or V-turn (overpass)-like fluctuation, which includes a downtrend and an uptrend. Each downtrend and the next uptrend would be identified as a segment of a U-turn. Besides, for a series of the same direction trend, the standard normal variable shows which trend is more drastic, and the others will be ignored as irrelevant trends.

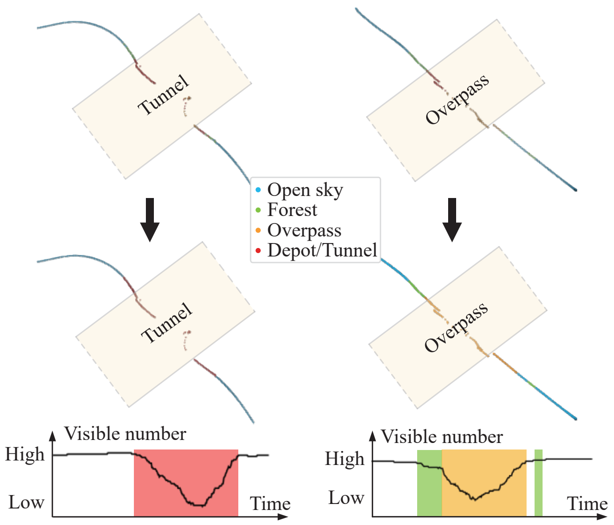

Figure 7 Results of inference after trend generation and U-turn segmentation

2.6 Evaluation parameter

The random forest (RF), support vector machine (SVM), and XGBoost were used as the baseline models to verify the effectiveness of the proposed method. Table 3 lists their hyperparameters.

Table 3 Hyperparameters of baseline model

Model	Name	Content	Model	Name	Content
Random forest	Number of trees	140	XGBoost	Booster	gbtree
	Criterion	Logarithmic loss		Learning rate	0.3
	Maximum feature	Square root		Number of trees	1
SVM	Kernel	Radial basis function		Maximum depth	6
	Gamma	Auto			
	Penalty term	15			

To assess the performance of the scene classification, we used three common evaluation metrics: precision (P), recall (R), and F1 score, to evaluate the classification performance for each scene type. Additionally, macro precision (macro-P), macro recall (macro-R), and macro F1 score (macro-F1) were employed to evaluate the overall classification performance across all scene types.

2.7 Scene length calculation

The length of each scene segment was computed as the cumulative travel distance along the GNSS trajectory between consecutive valid points classified as the same scene. Given a time-ordered sequence of GNSS latitude and longitude measurements, the geodesic distance between the last accepted point and the current point was calculated using a WGS84 geodesic model. This point-to-point distance represents the traveled distance along the vehicle trajectory. For each segment, the computed distance was added to the corresponding scene category based on the predicted label. In this way, the scene length was obtained as the sum of point-to-point distances, considering the curved road situation.

To address intervals with invalid or unreliable GNSS solutions, which frequently occur in tunnel environments, a speed-consistency check was applied to filter abnormal position jumps. For each candidate segment, an implied speed was calculated as the geodesic distance divided by the elapsed time between two points. This value was compared with the average horizontal speed reported by the GNSS receiver at these two points. If the implied speed exceeded the average reported speed by more than a fixed tolerance (0.03 m/s, corresponding to typical GNSS speed accuracy), the corresponding point was treated as unreliable and excluded from distance accumulation. In such cases, the last valid GNSS fix was retained, and distance computation resumed only when a subsequent point satisfied the consistency condition. As a result, distance contributions from intervals with missing or invalid positioning solutions were omitted, while the continuity of segment length estimation was preserved once valid measurements became available again.

3 Results and discussion

Figure 8 shows that “open sky”, “overpass”, and “tunnel” scenes are classified with high accuracy, while most misclassifications occur between “open sky” and “forest”, which reflects the gradual transition of GNSS signal characteristics along farm roads. “Overpass” and “tunnel” scenes exhibit distinct signal patterns and are therefore well separated from other scenes.

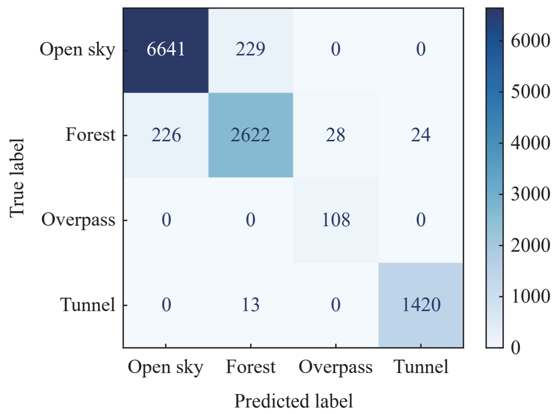

Figure 8 Result confusion matrix of the validation set

3.1 Feature comparisons

Tables 4 and 5 show the impact of different feature types on classification results. The results indicate that while using only the position output data achieves good performance for the “open sky” category, with an F1 score of 97.00 on the validation set, its performance is poor for the “overpass” category, with an F1 score of only 44.81. When combined with GNSS satellite distribution features, performance in the “overpass” category significantly improved, with an F1 score of 64.20 on the validation set, and the overall data with GNSS satellite statistical features also improved classification performance, with the macro F1 score increasing by 5.18 points. Combining position output data performance in the “overpass” category, the F1 score in the test set increased by 45.19 points, and the macro F1 score improved by 15.88 points. This demonstrates that GNSS satellite statistical features are highly effective for recognizing the “overpass” scene.

The combination of position output data, satellite distribution features, and statistical features achieved the best results in both the validation and test sets, particularly in the “overpass” and “tunnel” categories. The F1 scores on the test set for these categories were 83.48 and 98.26, respectively, confirming the effectiveness of the multi-feature fusion strategy. The combination of multiple features significantly improved classification accuracy and generalization ability, particularly when handling high complexity and data imbalance issues.

3.2 Method comparisons

Using all features as input data, Tables 6 and 7 present the results of the ablation experiments on different processing steps of classification and inference. The SVM, XGBoost, and random forest methods were used as baseline classifiers. SVM performed poorly across all categories, with F1 scores below 50.00 on both the validation and test sets, indicating that the complexity of the feature distribution was too high for SVM to distinguish between different categories. XGBoost performed moderately on the validation set but showed poor classification ability in recognizing "forest" and "overpass" scenes, with macro F1 scores of 60.51 and 77.99, respectively. XGBoost overfitted the feature data during gradient boosting, resulting in significant performance degradation on the test set due to distribution differences in the data. Among the baseline models, the random forest performed the best, with macro F1 scores improving by 15.56 and 12.13 on the validation and test sets, respectively, compared to XGBoost.

Table 4 Results of ablation experiments on different features (validation set)

Item	Open sky			Forest			Overpass			Tunnel			Overall		
	P/%	*R*/%	F1	*P*/%	*R*/%	F1	*P*/%	*R*/%	F1	*P*/%	*R*/%	F1	macro-*P*/%	macro-*R*/%	macro-F1
①	97.43	95.56	97.00	89.03	93.28	91.11	54.67	37.96	44.81	94.31	91.42	92.84	83.86	79.81	81.44
①+②	97.04	96.74	96.89	91.64	90.38	91.01	93.65	54.63	69.01	92.01	98.81	95.29	93.58	85.14	88.05
①+③	96.15	97.71	96.92	90.95	90.48	90.72	96.30	48.15	64.20	96.12	93.23	94.65	94.88	82.39	86.62
①+②+③	96.87	97.82	97.34	94.07	90.86	92.44	100.00	53.70	69.88	93.86	99.23	96.47	96.20	85.40	89.03

Note: ① is the position output data, ② is the satellite statistical feature, and ③ is the satellite distribution feature; same as below.

Table 5 Results of ablation experiments on different features (test set)

Item	Open sky			Overpass			Tunnel			Overall		
	P/%	*R*/%	F1	*P*/%	*R*/%	F1	*P*/%	*R*/%	F1	macro-*P*/%	macro-*R*/%	macro-F1
①	100.00	96.29	98.11	50.00	32.69	39.53	94.51	95.43	94.97	81.50	74.80	77.54
①+②	100.00	94.97	97.42	77.60	93.27	84.72	99.19	97.10	98.13	92.26	95.11	93.42
①+③	100.00	98.51	99.25	52.31	65.38	58.12	97.09	93.76	95.39	83.13	85.88	84.25
①+②+③	100.00	96.96	98.46	76.19	92.31	83.48	99.64	96.92	98.26	91.94	95.40	93.40

Table 6 Results of ablation experiments on different methods (validation set)

Method	Open sky			Forest			Overpass			Tunnel			Overall		
	P/%	*R*/%	F1	*P*/%	*R*/%	F1	*P*/%	*R*/%	F1	*P*/%	*R*/%	F1	macro-*P*/%	macro-*R*/%	macro-F1
SVM	0.00	0.00	0.00	25.64	100.00	40.81	0.00	0.00	0.00	0.00	0.00	0.00	6.41	25.00	10.20
XGBoost	93.70	98.33	95.96	90.42	34.48	49.93	19.78	49.07	28.19	51.83	98.67	67.96	63.93	70.14	60.51
RF	95.83	96.62	96.22	87.68	59.62	70.98	96.08	45.37	61.64	60.61	99.86	75.43	95.05	75.37	76.07
SMOTE+RF	95.58	96.97	96.27	90.38	70.97	79.51	68.83	49.07	57.30	71.82	99.58	83.45	81.65	79.15	79.13
Rolling+RF	96.73	97.26	97.00	92.02	82.72	87.13	96.55	51.85	67.47	81.70	99.09	89.56	91.75	82.73	85.29
Rolling+SMOTE+RF	96.87	97.82	97.34	94.07	90.86	92.44	100.00	53.70	69.88	93.86	99.23	96.47	96.20	85.40	89.03
Rolling+SMOTE+RF+Inference	96.71	96.67	96.69	90.31	92.21	91.25	100.00	100.00	100.00	100.00	95.95	97.93	96.75	96.21	96.48

Note: SVM is the support vector machine; RF is the random forest classification; SMOTE is the synthetic minority over-sampling technique; Rolling is handled for sliding window; Inference is tracked satellite number-based inference; same as below.

Table 7 Results of ablation experiments on different methods (test set)

Method	Open sky			Overpass			Tunnel			Overall		
	P/%	*R*/%	F1	*P*/%	*R*/%	F1	*P*/%	*R*/%	F1	macro-*P*/%	macro-*R*/%	macro-F1
SVM	0.00	0.00	0.00	0.00	0.00	0.00	0.00	0.00	0.00	0.00	0.00	0.00
XGBoost	100.00	90.32	94.91	53.29	77.88	63.28	61.80	97.89	75.77	71.70	88.70	77.99
RF	100.00	90.93	95.25	72.50	83.65	77.68	97.87	97.01	97.44	90.12	90.53	90.12
SMOTE+RF	100.00	75.78	79.13	62.50	86.54	72.58	98.90	94.99	96.90	97.13	85.77	85.24
Rolling+RF	100.00	91.61	95.62	75.00	92.31	82.76	98.40	97.19	97.79	91.13	93.70	92.06
Rolling+SMOTE+RF	100.00	96.96	98.46	76.19	92.31	83.48	99.64	96.92	98.26	91.94	95.40	93.40
Rolling+SMOTE+RF+Inference	100.00	95.38	97.64	81.89	100.00	90.04	100.00	99.56	99.78	93.96	98.31	95.82

After oversampling the training set using SMOTE, the classification performance for the "forest" category significantly improved, with accuracy, recall, and F1 scores on the validation set increasing by 2.70%, 11.35%, and 8.53, respectively. SMOTE effectively enriched the minority class sample set and expanded the data boundaries for this category, enhancing the model's performance. After applying the sliding window to process the features, the random forest model's macro F1 score on the validation set increased by 9.22 points. The classification accuracies for the "open sky", "forest", "overpass", and "tunnel" categories reached 96.73%, 92.02%, 96.55%, and 81.70%, respectively, with the recall rates for the "forest" and "overpass" categories increasing by 23.10% and 6.48%, respectively. The sliding window effectively captured the gradual changes in positioning features at scene boundaries and aided in identifying scene transitions. The random forest model trained on oversampled and sliding window-processed data achieved the best overall performance, with a macro F1 score of 89.03 and all evaluation metrics approaching or exceeding 90%.

This demonstrates the model's adaptability in handling complex scenes and class imbalance problems.

With subsequent inference, the performance in the "overpass" category improved significantly, with the recall rate on the validation set surging from 53.70% to 100.00% and the F1 score increasing from 69.88 to 100.00. Furthermore, performance in the "tunnel" category also improved, with the macro F1 score on the test set reaching 97.93, the highest among all methods. These results indicate that the introduction of U-turn segmentation can further improve classification performance, particularly in "overpass" and "tunnel" scenes.

3.3 Analysis and discussion

Following classification and inference, the segment lengths for each scene type can be determined based on the validation set. The length of "open sky" is 6619.36 meters; "forest" is 1832.04 meters; "overpass" is 70.24 meters; and "tunnel" is 54.58 meters. Based on the type and length of the segments, the positioning accuracy and reliability were assessed to guide the selection of appropriate sensors and the route planning for unmanned agricultural machines. As shown in Figure 9, in the open sky scene, positioning accuracy is high and reliable, and using GNSS in combination with a relatively low-cost inertial navigation system (INS) can meet positioning requirements[21]. In the forest scene, positioning accuracy fluctuates, sometimes providing accurate results and other times not, so it is recommended to use a medium-precision INS to handle long, dense forested areas in summer. For the overpass scene, there are positioning results, but the accuracy is low. Given the short distance of such segments, a more expensive INS may be needed to meet pure inertial navigation positioning requirements within 1 min. In the tunnel scene, GNSS positioning fails, and lidar-based positioning is ineffective due to the lack of environmental features[22]. In such cases, using a high-precision INS with long-term stability or alternative methods like visual positioning is recommended, or an alternative route should be considered.

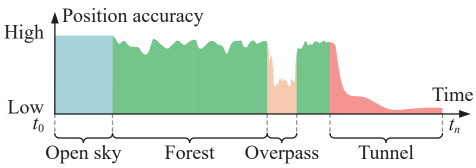

Figure 9 Scene segments diagram of farm roads

4 Conclusions and future work

The main contributions of this study in the field of unmanned agricultural machinery navigation are mainly as follows:

Considering the precision defect of GNSS used in agricultural machinery positioning on the farm road, China's farm roads are regularly divided into four categories, including open sky, forest, overpass, and tunnel, to support manager decisions and positioning algorithms.

1) In order to describe the occlusions of GNSS satellite signals in different scenes, satellite statistical features and satellite distribution features were innovatively extracted to reveal the characteristics of sky occlusions and improve classification accuracy. The overall F1 score of the test set classification was improved by 15.86 compared to using the positioning output data.

2) According to the features of overpass and tunnel scenes, a trend generation and U-turn detection segment inference method is proposed to identify the start and end of scenes and unify the discontinuous classification within the segment, and the scene boundary is well identified.

3) The study conducted comprehensive data collection and analysis in a real agricultural machinery working environment. The results show that the proposed detection method has high accuracy on farm roads, providing support for efficient navigation and route planning of unmanned agricultural machinery.

The method used in this study, due to the limitations of experimental data collection conditions, is primarily applicable to scenarios with preset environments or repeatable movement routes, usually within confined areas. The diversity of data in this study is insufficient. The tunnel scenes do not include underpasses, mountain tunnels, etc., and the overpass scenes are limited, lacking data for different bridge widths and heights. Considering the diversity of farm road environments in different regions, expanding the dataset to include data from various regions and using time-series deep learning algorithms could enhance the applicability of farm road scene recognition, making it feasible for broader geographic areas. In addition, since there is a time difference between the GNSS antenna receiving the signal and achieving the tracking, the result of inference based on tracked satellite numbers detection usually exceeds the scene coverage, resulting in a lower recall rate. Future research could focus on incorporating more detailed quantitative measurements and refining definitions for certain scene types, such as transitions around overpasses and forests during winter. Additionally, a deeper investigation into the positioning accuracy and reliability for each scene type would provide more precise and scientific guidance for subsequent applications.

Acknowledgements

This work was financially supported by the National Key R&D Program of China (Grant No. 2021YFB3901300).

[References]

[1] Zhou W J, Liu L Z, Liu R Q, Chen F, Yang L Y, Qin L F, et al. Precise mapping of linear shelterbelt forests in agricultural landscapes: A deep learning benchmarking study. Forests, 2026; 17(1): 91.

[2] Luo X W, Hu L, He J, Zhang Z G, Zhou Z Y, Zhang W Y, et al. Key technologies and practice of unmanned farm in China. Transactions of the CSAE, 2024; 40: 1–16. (in Chinese)

[3] Luo X W, Liao J, Hu L, Zhou Z Y, Zhang Z G, Zang Y, et al. Research progress of intelligent agricultural machinery and practice of unmanned farm in China. Journal of South China Agricultural University, 2021; 42: 8–17. (in Chinese)

[4] Yao Z X, Zhao C J, Zhang T H. Agricultural machinery automatic navigation technology. iScience, 2024; 27(2): 108714.

[5] Hu L, Wang Z M, Wang P, He J, Jiao J K, Wang C Y, et al. Agricultural robot positioning system based on laser sensing. Transactions of the CSAE, 2023; 39: 1–7. (in Chinese)

[6] Kowalczyk W Z, Hadas T. A comparative analysis of the performance of various GNSS positioning concepts dedicated to precision agriculture. Reports on Geodesy and Geoinformatics, 2024; 117(1): 11–20.

[7] Kou R X, Yang B S, Dong Z, Liang F X, Yang S W. Mapping the spatio-temporal visibility of global navigation satellites in the urban road areas based on panoramic imagery. International Journal of Digital Earth, 2021; 14: 807–820.

[8] Xu H S, Hsu L T, Lu D B, Cai B G. Sky visibility estimation based on GNSS satellite visibility: An approach of GNSS-based context awareness. GPS Solutions, 2020; 24(2): 59.

[9] Kim D, Youn J, Kim T, Kim G. 3D grid-based global positioning system satellite signal shadowing range modeling in urban area. Sensors and Materials, 2019; 31(11): 3835–3848.

[10] Kou R X, Tan R C, Wang S Y, Yang B S, Dong Z, Yang S W, et al. Satellite visibility analysis considering signal attenuation by trees using airborne laser scanning point cloud. GPS Solutions, 2023; 27: 64.

[11] Zhang T, Cai B G, Lu D B, Wang J, Xiao Y. Train localization environmental scenario identification using features extracted from historical data. In: China Satellite Navigation Conference (CSNC 2021) Proceedings, Springer, 2021; pp.12–21. doi: 10.1007/978-981-16-3138-2_2.

[12] Chen W J, Zhu F, Guo F, Zhang X H. GNSS signal characteristics analysis in different water layers and navigation context clustering. Geomatics and Information Science of Wuhan University, 2024; 49: 139–145. (in Chinese)

[13] Liang Y J, Zhou K, Wu C C. Environment scenario identification based on GNSS recordings for agricultural tractors. Computers and Electronics in Agriculture, 2022; 195: 106829.

[14] Xia Y, Pan S G, Gao W, Yu B G, Gan X L, Zhao Y, et al. Recurrent neural network based scenario recognition with multi-constellation GNSS measurements on a smartphone. Measurement, 2020; 153: 107420.

[15] Groves P, Martin H F S, Voutsis K, Walter D. Context detection, categorization and connectivity for advanced adaptive integrated navigation. In: Proceedings of the 26th International Technical Meeting of the Satellite Division of The Institute of Navigation (ION GNSS+2013), 2013; pp.1039-1056.

[16] Feriol F, Vivet D, Watanabe Y. A review of environmental context detection for navigation based on multiple sensors. Sensors, 2020; 20(16): 4532.

[17] Wang T H, Chen B, Zhang Z Q, Li H, Zhang M. Applications of machine vision in agricultural robot navigation: A review. Computers and Electronics in Agriculture, 2022; 198: 107085.

[18] Attia D, Meurie C, Ruichek Y, Marais J. Counting of satellites with direct GNSS signals using Fisheye camera: A comparison of clustering algorithms. In: 2011 14th International IEEE Conference on Intelligent Transportation Systems - (ITSC 2011), Washington: IEEE, 2011; pp.7–12. doi: 10.1109/ITSC.2011.6082955.

[19] Chawla N V, Bowyer K W, Hall L O, Kegelmeyer W P. SMOTE: Synthetic minority over-sampling technique. Journal of Artificial Intelligence Research, 2002; 16: 321–357.

[20] Breiman L. Random forests. Machine Learning, 2001; 45: 5–32.

[21] Feng Y H, Huang G W, Wang M F, Li X, Li Z H, Li H, et al. GNSS/MEMS INS tightly coupled algorithm for agricultural machinery navigation enhanced by random forest-based behavioral state awareness. Computers and Electronics in Agriculture, 2026; 242: 111350.

[22] Zhen W K, Scherer S. Estimating the localizability in tunnel-like environments using LiDAR and UWB. In: 2019 International Conference on Robotics and Automation (ICRA), Montreal: IEEE, 2019; pp.4903–4908. doi: 10.1109/ICRA.2019.8794167.